*Desalination and Water Treatment*
www.deswater.com
doi: 10.5004/dwt.2020.25084

180 (2020) 185–192
March

# Identification of natural wastes for application in water treatment

Redouane Ouafi*, Zakia Rais, Mustapha Taleb

*Laboratory of Electrochemistry Engineering, Modeling and Environment, Faculty of Science, Dhar El Mahraz, Sidi Mohamed Ben Abdellah University, Fez, Morocco, emails: redouane.ouafi@usmba.ac.ma (R. Ouafi), zakia.rais@usmba.ac.ma (Z. Rais), mustaphataleb62@yahoo.fr (M. Taleb)*

Received 30 May 2019; Accepted 23 October 2019

**ABSTRACT**

Minimizing wastes and making the most of natural resources are the aims of the circular economy. Natural wastes were employed as abundant and inexpensive materials for wastewater treatment. In this context, snail shell powder (SSP) and pine cone powder (PCP) were studied for their ability to remove pollutants from wastewater, especially heavy metals. For the characterization of adsorbents, scanning electron microscope (SEM), Fourier transform infrared spectroscopy (FTIR), X-ray diffraction (XRD) analysis and measurement of point of zero charge (PZC) were carried out. The PCP crystallinity index was evaluated by the peak height and deconvolution method. The apparent crystallite size was estimated using the Scherrer equation. The SEM micrographs showed the irregular morphology of their particles and the roughness of their surfaces. FTIR analysis allowed the identification of functional groups present on the surface of both adsorbents, mainly related to their abatement capacity. XRD analysis showed that SSP was a calcium carbonate compound in the aragonite mineralogical form. PCP was mainly constituted of cellulose in amorphous and crystalline phase. The PCP deconvolution results indicate that the crystalline peak (200) was directly related to crystallite size. The PZC results were used to explain general connections among points of zero charges and cation exchange capacity of the adsorbents. The PZC values were 7.97 and 5.62 for SSP and PCP, respectively. This work highlights the applicability of the SSP and PCP as available and low-cost natural wastes that can be involved in an efficient and economically appealing wastewater treatment process.

*Keywords:* Circular economy; Snail shell; Pine cone; Waste management; Wastewater treatment; Heavy metals

## 1. Introduction

The growth of industrial activity has caused the discharge of large quantities of wastewater containing different inorganic and organic compounds. These pollutants include dyes, phenols, oil, toxic salts and heavy metals [1]. Their release in the environment constitutes a serious threat for human health and the entire biological system due to their toxic nature [2]. The treatment of polluted wastewater hence remains a topic of scientific interest that requires intensive efforts to be solved. Therefore, the development of new efficient technologies, easy to implement deserves special attention.

A scrutiny of literature indicates a growing interest in the employment of low-cost adsorbents [3]. Indeed, these available and cheap materials can be involved in an efficient and economically appealing process of decontamination. Owing to their numerous advantages, they have been extensively used as a promising alternative to traditional physicochemical methods for wastewater treatment.

Various materials have been investigated as adsorbents to remove different types of pollutants from aqueous solutions. It includes mineral materials, synthetic organic materials, agriculture wastes, industrial by-products and natural residues [4–6]. Among the used materials, snail shell is an

* Corresponding author.

abundant, low-cost and natural waste material that can be used in polluted effluents treatments. The snail is relished as gourmet food in a number of countries such as Morocco. It provides an easily harvested source of protein for the local communities, discarding the shells as wastes [7]. The use of these shells as adsorbents transforms a waste material into a potential useful resource. On the other hand, large quantities of pine cones are produced as agricultural by-products throughout the world [8]. The cones are the reproductive organs of the pines and other conifers. Each cone is composed of a large number of scales carrying seeds. They are easily available waste that can be used as a potent decontamination tool [9].

In analogy with the incessant search for cheaper, feasible and proficient products for the removal of various pollutants from wastewater, snail shell powder (SSP) and pine cone powder (PCP) have been studied. Our investigation aims to assess their potential application in wastewater treatment. In this regard, the physicochemical characterization of these natural wastes was explored by using scanning electron microscope (SEM), Fourier transform infrared spectroscopy (FTIR) and X-ray diffraction (XRD) analysis. The point of zero charge (PZC) of both adsorbents was studied. The PCP crystallinity index was evaluated by the peak height and deconvolution method. The crystallite size was estimated using the Scherrer equation. The characterization results would contribute to a better understanding of the potential use of SSP and PCP for the removal of pollutants, such as heavy metals, from wastewater.

## 2. Materials and methods

### 2.1. Adsorbent preparation

The snail shells (*Helix aspersa*) were collected from street hawker in Fez, Morocco. They were washed several times with tap water and then oven-dried at 80°C for 2 h. The materials were crushed in an agate mortar; impurities such as flesh were removed and then washed several times with distilled water. Finally, the product was oven-dried at 100°C for 12 h.

Pine cones (*Pinus halepensis*) were collected from the peri-urban forests in Fez, Morocco. The cone scales were removed and extensively rinsed with distilled water to remove impurities. The materials were then oven-dried at 60°C for 48 h.

The dried natural wastes were ground to a fine powder using a food-processing blender. The resulting PCP and SSP were sieved through a range of sieves between 20 and 800 μm. The different resulting powders were collected for further experimental use.

### 2.2. Physicochemical characterization

The FTIR analysis was recorded using Bruker (Germany) FTIR spectrophotometer model Vertex 70, in the range of 400–4,000 $cm^{-1}$, using ATR mode, 16 scans were accumulated at a resolution of 4 $cm^{-1}$.

The scanning electron microscopy is a powerful technique that can be used to investigate the surface morphology of adsorbents. The SEM analysis was carried out by an environmental scanning electron microscopy equipped with an EDAX probe, model QUANTA 200 coupled with energy dispersive spectroscopy (EDS) under a vacuum of 90 Pa.

The X-ray diffraction (XRD) pattern of the powdered samples was obtained using a PAN-Critical X'Pert Pro X-ray diffractometer equipped with a Cu-K$\alpha$ monochromatic source (1.54 Å). Operating at a voltage of 40 kV, a step size of $2\theta = 0.071°$ and a filament current of 40 mA. The diffraction pattern was recorded with continuous scanning from 10° to 90° at a scan step time of 45.08 s for SSP and from 5° to 40° at a scan step time of 90.17 s for PCP.

The solid addition method was used to determine the PZC of the adsorbent [10,11]. A mass of 0.5 g of the material was brought into contact with a volume of 45 mL of the $KNO_3$ (0.01 N) solution. The initial pH ($pH_i$) values of the solutions were adjusted ranging from 2 to 10 using KOH (0.1 N) and $HNO_3$ (0.1 N) solutions. Afterwards, the total volume of the solution was made to 50 mL by adding $KNO_3$ solutions. The mixtures were shook at 200 rpm for 24 h in an orbital shaker, and the final pH ($pH_f$) values of the supernatant liquid were recorded. The difference between the initial and final pH values ($\Delta pH = pH_i - pH_f$) was plotted against the $pH_i$. The point of intersection of the resulting curve at $\Delta pH = 0$ was considered as the PZC.

The particle size analysis was conducted using an AS 200 RETSCH (Germany) analytical sieving machine, through a series of sieves in accordance with ISO3310-1. A sample of 200 g of the material was sieved for 40 min at an amplitude of 1.8 mm; the resulting refusal is collected and weighed.

## 3. Results

### 3.1. FTIR analysis

FTIR analysis of the SSP was realized in order to determinate the functional groups on the material surface. The infrared spectrum in Fig. 1a reveals the presence of the characteristic fundamental vibration modes of the carbonate ions ($CO_3^{2-}$), identified by the main absorption bonds $_3$ = 1,447.40 $cm^{-1}$, $\nu_1$ = 1,082.62 $cm^{-1}$, $\nu_2$ = 854.19 $cm^{-1}$ and $\nu_4$ = 712.33 $cm^{-1}$. Indeed, carbonate ions molecules are known to present four normal modes of vibration peaks: $\nu_1$, symmetric stretching; $\nu_2$, out of plane bending; $\nu_3$, doubly degenerate planar asymmetric stretching; and $\nu_4$, doubly degenerate planar bending [12].

Furthermore, the existence of FTIR bonds from 1,600 to 1,400 $cm^{-1}$, from 1,081 to 1,083 $cm^{-1}$ and at 854 $cm^{-1}$ indicates the aragonite phase of calcium carbonate. Compared with the infrared spectrum of calcite showing a simple bond, aragonite presents a double peak at 699.60 and 712.33 $cm^{-1}$. The bonds at 1,786.70 $cm^{-1}$ are assigned to the combination of symmetric stretching $\nu_1$ and doubly degenerate planar bending $\nu_4$.

The obtained FTIR spectral data were in accordance with the common characteristics of carbonate groups generally found in calcium carbonate compounds as confirmed by other studies [13–16]. Moreover, the carbonyl (C=O) group present in SSP is expected to act as an active group for the fixation of toxic metal ions [17].

FTIR analysis also concluded the predominant aragonite phase of calcium carbonate in the SSP. These findings were further justified through XRD analysis shown in Fig. 3.

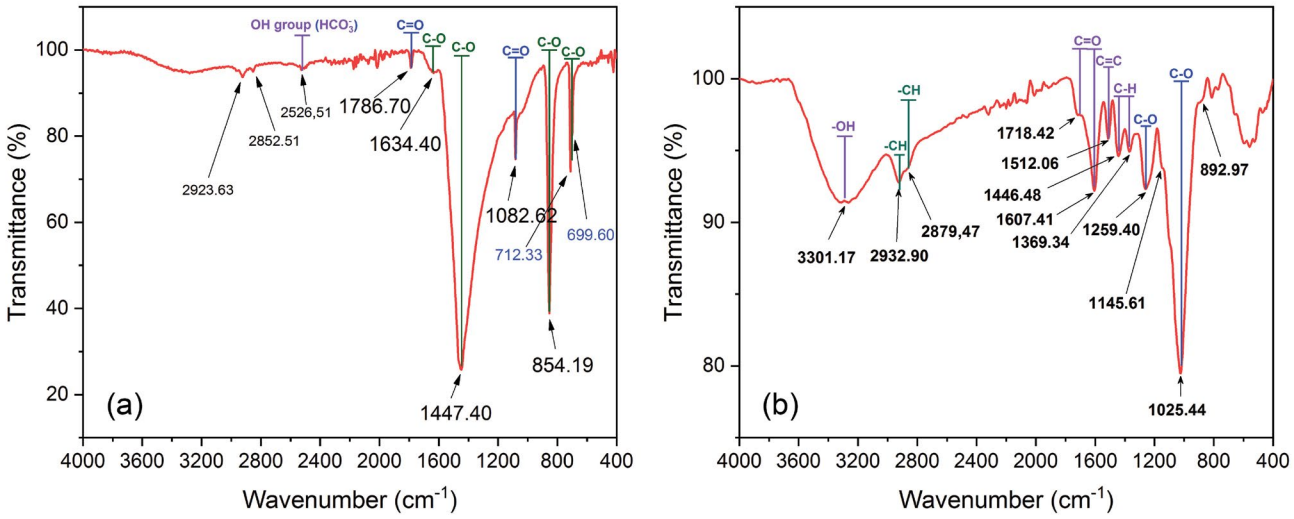


Fig. 1. FTIR spectra: (a) SSP; (b) PCP.

The FTIR spectra of PCP given in Fig. 1b show a bond at 3,301.17 $cm^{-1}$ corresponding to O–H stretching vibration. This bond is probably attributed to hydrogen bending of the hydroxyl and carboxyl group linked in cellulose, lignin and adsorbed water.

The double peaks observed at 2,932.9 and 2,879.47 $cm^{-1}$ are possibly related to the symmetric and asymmetric stretching of aliphatic chains C–H, respectively, particularly due to methyl ($CH_3^-$) and methylene ($-CH_2^-$) groups of side chains. The peaks at 1,718.42 and 1,607.41 $cm^{-1}$ could be attributed to C=O vibration due to the carboxylic and carboxylate form, respectively. The peak at 1,512.06 $cm^{-1}$ may be ascribed to the presence of aromatic rings with C=C bonds and can be assigned to lignin. The peak at 1,259.40 $cm^{-1}$ corresponds to C–O vibration bond from the carboxylic acids or stretching vibration of O–H from phenols. The peak present at 1,025.44 $cm^{-1}$ may be assigned to C–O ether and alcohol, especially in cellulosic compounds.

Peaks in 900–800 $cm^{-1}$ area would be attributed to C–H aliphatic or aromatic bonds. The infrared spectrum reveals the presence of the characteristic functional groups reported in other studies [18–24].

The performed investigations on PCP showed that they are generally composed of cellulose, hemicellulose, lignin and extractives as it was reported in previous study [25–27]. PCP contains functional groups such as ketones, hydroxyl, carboxyl and phenol. These functional groups are strongly involved in the pollutant particles binding. Their presence would provide to this material a great adsorptive potential for the treatment of heavy metal from aqueous solutions. Their involvement in heavy metals adsorption was reported in various research works [21,28,29].

### 3.2. SEM analysis

The surface morphology of the samples was observed using SEM at 15 kV accelerating voltage. The SEM images are shown in Fig. 2a. The surface of SSP consists of condensed agglomerates made up of small particles and many spaces. Furthermore, the visible rough and irregular surface of the material revealed the porous characteristic. This surface property could be considered as a factor favoring the adsorption of pollutants by an ion exchange phenomenon leading to the fixation of cationic or anionic particles for example. These results are in accordance with those found in previous studies [30,31].

The SEM of PCP shown in Fig. 2b presents irregular particles with medium outline relief and containing varieties of interstice. The particles of PCP seem to have rough texture and a porous surface. This surface nature offers a high surface area and could strongly contribute to the adherence of the pollutant as previously reported [21].

### 3.3. XRD analysis

The crystalline structure of the SSP can be observed by analyzing the XRD patterns as shown in Fig. 3. The main diffraction peaks are identified in the range of $2\theta = 25°–55°$. The most representative peaks were located at $2\theta = 26.23°$, 27.22°, 33.14°, 36.17°, 37.90°, 45.88°, 48.42° and 52.47°. These peaks were assigned to the aragonite crystal form as deduced from the comparison with the data file ICDD reference code 96-901-5426. The XRD patterns of the SSP were in accordance with previous results reporting based calcium carbonate aragonite materials [10,14,32].

The calcium carbonate constituting the snail shell exhibits usually two mineralogical forms, calcite and aragonite. The calcite crystallizes in the rhomboidal system, while aragonite crystallizes in the orthorhombic system where each calcium ion is coordinated with nine oxygen ions and each oxygen ion with three calcium ions. The calcium ions have an approximately hexagonal compact arrangement. Calcium in both forms can be partly replaced by other elements. In aragonite, Ca is replaced by strontium (Sr) and barium (Ba), while in calcite it is likely replaced by magnesium (Mg) and manganese (Mn). Indeed, we can assume that the strontium can naturally integrate the aragonite lattice since this atom is divalent, and has an ionic radius close to calcium. These

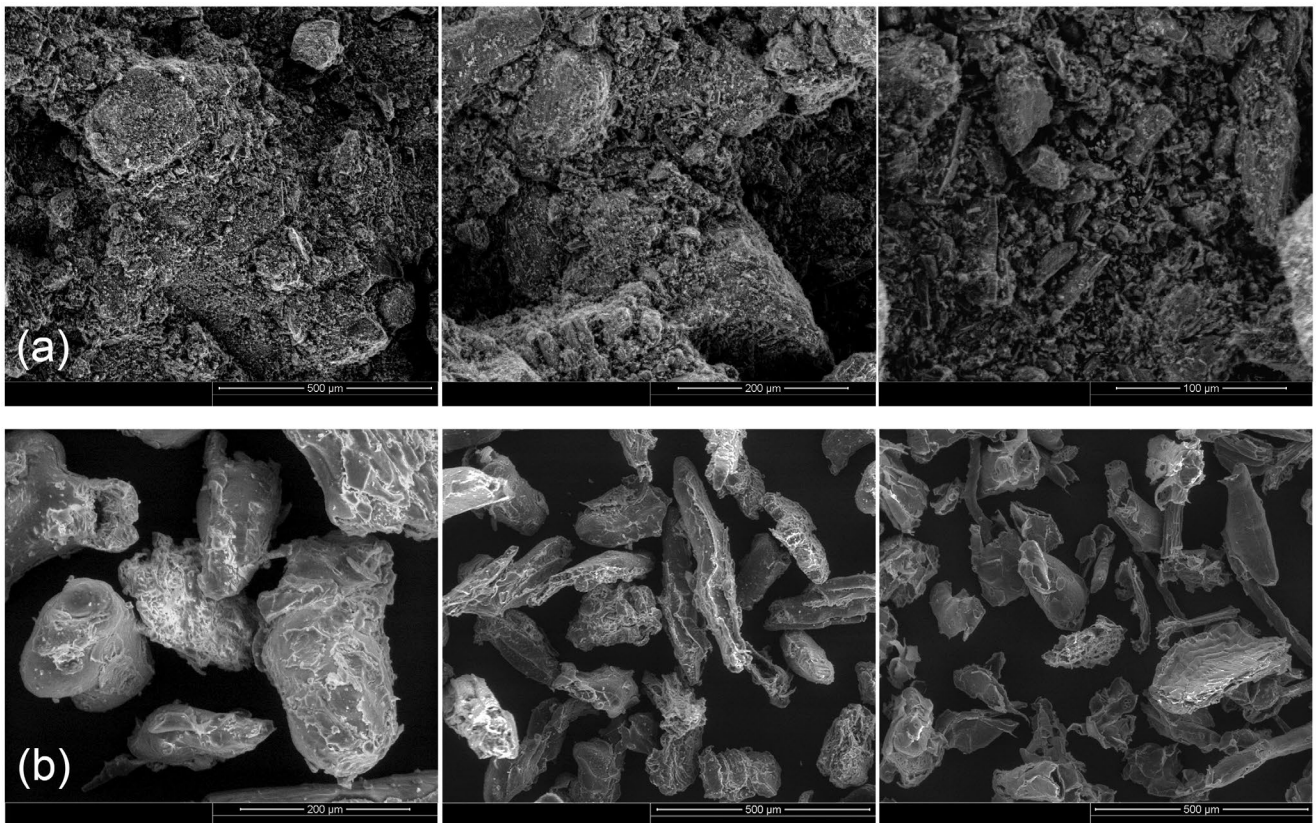


Fig. 2. SEM images SEM: (a) SSP; (b) PCP.

findings are in agreement with results reported in previous studies [16,30,33]. It is noteworthy that no additional peak was observed in the XRD patterns. This demonstrates the high purity of aragonite polymorph of calcium carbonate in the SSP.

The X-ray diffractogram of PCP is shown in Fig. 4a. The four peaks located at 2θ angles of 15.09°, 16.25°, 22.21° and 34.47° are characteristic of cellulose I [34], and are used for the structural analysis and comparison. Native cellulose is known to be a mixture of two distinct crystalline forms, namely celluloses Iα (triclinic) and Iβ (monoclinic), whose fractions vary depending on the origin of the cellulose sample [35,36]. XRD spectrum of PCP is similar to that of cellulose Iβ characterized by two main peaks and a broad amorphous background bond. The peak intensities and the peak broadening are species dependent. Peaks at 2θ = 15.09° and 16.25° merged into a broad bond, which is consistent with the literature [24,26]. The most prominent peak observed at 2θ = 22.21° was assigned to the (200) plane from the cellulose crystalline phase. Besides this phase, an amorphous phase is located at 2θ = 18.28° area and mainly corresponds to lignin, associated to the cellular wall; this compound confers mechanical strength to the wood. The decrease of its concentration leads to the increase of the crystalline fraction [25].

The empirical crystallinity index (CrI) = 51.32 % was estimated using the Segal equation (Eq. (1)) [37], that is, the ratio of crystalline cellulose intensity ($I_c$–$I_{am}$) to total intensity ($I_c$) at 2θ = 22.21°, where $I_{am}$ is the intensity of the amorphous

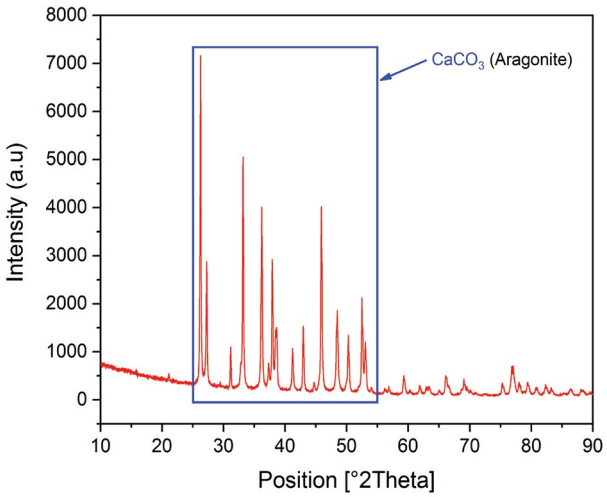


Fig. 3. X-ray diffractogram of the SSP.

cellulose phase at 2θ = 18.28° which corresponds to the minimum position of the diffraction profile. Fig. 4a shows an example of the crystalline and amorphous peaks used in this equation.

$$\mathrm{CrI}(\%) = \frac{I_c - I_{am}}{I_c} \times 100 \quad (1)$$

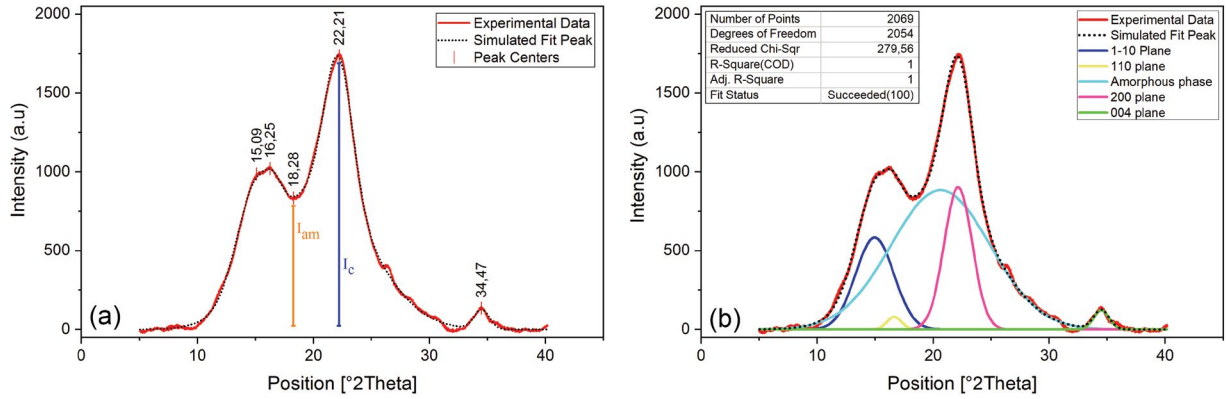


Fig. 4. XRD patterns of PCP for calculating CrI: (a) by the intensity method; (b) by the area method.

The deconvolution method was used for the separation of the crystalline phase from the amorphous background. As shown in Fig. 4b individual peaks were fitted by Gaussian functions. For this purpose, Peak Analyzer with program Origin was used and interactions continued until the fit convergence, which corresponds to an $R^2 = 0.99$. The fitting curve matches the experimental curve very well; therefore, the use of this function is a good approach.

After deconvolution, five bonds have been assumed (Table 1). This result was reported in many other cases [26,38–40]. The crystallinity ($X_c$ = 36.65%) was calculated by Eq. (2) [24]:

$$X_c = \frac{S_c}{S_c + S_{am}} \times 100 \quad (2)$$

where $S_{am}$ is the amorphous integrated area, and $S_c$ is the sum of the integrated areas of the crystalline adjusted peaks designated as (1–10), (110), (200) and (004) in Fig. 4b.

The calculated value of CrI is greater than the value obtained for $X_c$. It is most likely because the CrI calculated using the Segal method is a rough approximation of the percentage of crystalline part in whole cellulose mass. Indeed, this approach only considers the crystallinity part present in the (200) plane, neglecting the contributions of the other crystalline planes. The crystallinity index Segal's method is not able to reflect the degree of biomass crystallinity; however, it provides a comparison parameter. Similar results have been reported by Poletto et al. [26] and Ornaghi Júnior et al. [40].

The average size of crystallite was calculated from the Scherrer equation (Eq. (3)) [41]. The method is based on width at half height of the diffraction patterns obtained in the X-ray reflected crystalline region. The crystalline size ($L_{hkl}$) was determined using the diffraction pattern obtained from deconvolution approach.

$$L_{hkl} = \frac{k\lambda}{\beta \cos\theta} \quad (3)$$

where $k$ is a dimensionless number known as the Scherrer constant with a value of 0.94, $\lambda$ is the X-ray wavelength (0.154 nm for Cu K$\alpha$ radiation), $\beta$ in radians is the full width half maximum of the diffraction peak (FWHM) and $\theta$ is the corresponding Bragg angle.

Information about average crystallite size was calculated from this method using the Scherrer formula. Among the five reflections, the crystalline peak (200) is the clearest and the best able to determine the lateral dimension of the crystallite. The crystalline peak (200) was directly related to crystallite size and calculated to be 2.97 nm in this investigation. The value of the crystalline size was similar to that found by Poletto et al. [26] for *Eucalyptus grandis*, *Mezilaurus itauba* and *Pinus elliottii*.

### 3.4. PZC determination

The PZC is an important feature that determines the pH at which the surface of the adsorbent has a net electrical neutrality [42]. At this value, the acidic or basic functional

Table 1
Peak list of PCP after deconvolution

| Peak index | Peak area | β (°) | β (rad[a]) | Height | 2θ | $L_{hkl}$ (nm) | $X_c$ (%) | CrI (%) |
|---|---|---|---|---|---|---|---|---|
| 1 (1–10) | 2,403.022 | 3.869 | 0.068 | 583.435 | 14.960 | 2.164 | | |
| 2 (110) | 127.825 | 1.495 | 0.026 | 80.301 | 16.644 | 5.608 | | |
| 3 (amorphous phase)[b] | 9,458.347 | 10.054 | 0.175 | 883.901 | 20.634 | 0.839 | 36.65 | 51.32 |
| 4 (200) | 2,738.012 | 2.852 | 0.050 | 901.793 | 22.152 | 2.969 | | |
| 5 (004) | 203.969 | 1.566 | 0.027 | 122.383 | 34.496 | 5.555 | | |

[a]1° × π/180 = 0.01745 rad.
[b]Band assigned to amorphous phase.

groups no longer contribute to the pH of the solution. The adsorption of the cations will be more favorable at pH higher than PZC.

The PZC of SSP was determined to be 7.97 as presented in Fig. 5a. The PZC value of this adsorbent was similar to that obtained in previous works, such as 8.20 for natural calcite and 7.9 for snail shell [10,43].

At pH = 7.97 the quantity of negative charges on the SSP surface sites is equal to the quantity of positive charges. Therefore, at solution pH lower than 7.97, the SSP surface is predominated by positive charges and could interact with negative species.

At pH higher than 7.97, the SSP surface is predominated by negative charges and could interact with metal positive species as shown in Fig. 6.

The hydrolysis reaction of calcite ($CaCO_3$) could be used to elucidate the surface reaction of the SSP at different pH values. The reaction leads to the production of the following chemical species, $CO_3^{2-}$, $HCO_3^-$, $CaOH^+$, $Ca^{2+}$, $CaHCO_3^+$. Some reactions for the cationic and anionic species are as follows [44]:

$$CaCO_3 \leftrightarrow Ca^{2+} + CO_3^{2-}$$

$$CO_3^{2-} + H_2O \leftrightarrow HCO_3^- + OH^-$$

$$Ca^{2+} + HCO_3^- \leftrightarrow CaHCO_3^+$$

$$Ca^{2+} + OH^- \leftrightarrow CaOH^+$$

Thus, considering the hydrolysis reaction of calcite and PZC of SSP, it seems that cationic species such as $Ca^{2+}$, $CaHCO_3^+$, and $CaOH^+$ overcome at pH < 7.97 and offer hence a positive charge to the SSP surface. At pH > 7.97, the negative species such as $CO_3^{2-}$, $HCO_3^-$ prevails.

The PZC of PCP was determined to be 5.62 as illustrated in Fig. 5b. Depending on the solution pH, the organic functional groups on the PCP surface could acquire a negative or positive charge. At pH values lower than PZC, the sites will be associated with a proton to become positively charged, while at pH values greater than the PZC, the groups are mainly in dissociated form and acquire a negative charge. At pH equal to PZC, the amount of negative charge on the adsorbent surface equals the amount of positive charge as represented in Fig. 6.

The PCP surface contains carboxylic groups (–COOH) as revealed by the FTIR analysis. At pH > PZC, the carboxyl group turns into –COO– offering a negative charge to the PCP surface. This latter becomes attractive to cationic species such as heavy metals and cationic dye. The same phenomenon occurs with –OH and $–NH_2$ groups according to the following reactions:

$$S–COO^- + M^{n+} \rightarrow S–COOM^{(n-1)}$$

$$S–O^- + M^{n+} \rightarrow S–COOM^{(n-1)}$$

$$S–N^{2-} + M^{n+} \rightarrow S–NM^{(n-2)}$$

where S refers to the adsorbent surface and M to heavy metals.

Similar findings were obtained by Zou et al. [45] in a study dealing with the treatment of methylene blue bearing aqueous solutions by *Pinus tabuliformis* sawdust. Munagapati et al. [46] reported in a further work the applicability of a*cacia leucocephala* bark powder as an alternative biosorbent material for removal of Cu(II), Cd(II) and Pb(II) ions from aqueous solutions.

### 3.5. Particle size analysis

The particle size distribution is an important physical characteristic that needs to be analyzed. The milling of the solid is an initial pretreatment of the sample to obtain the best size for the further application. This process requires high-energy consumption. Thus, adequate particle size of the solid provides an economic advantage for its use in adsorption, for example.

Particle size distribution curve obtained through the sieve analysis is presented in Fig. 7. It is noteworthy that approximately 39.5% and 44.5% of PCP and SSP particles, respectively, presented a size of 300 μm which represents the

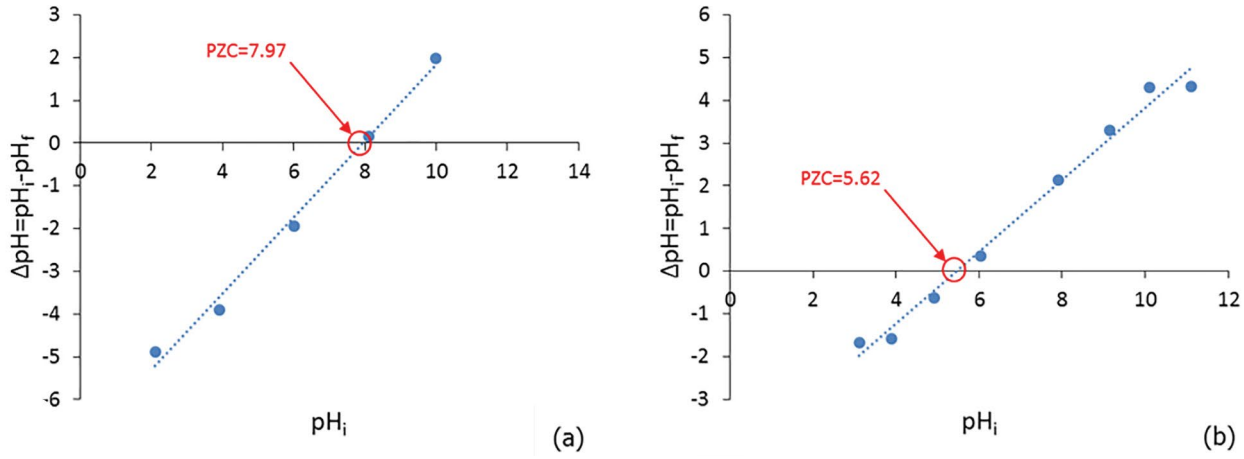


Fig. 5. Point of zero charge: (a) SSP; (b) PCP.

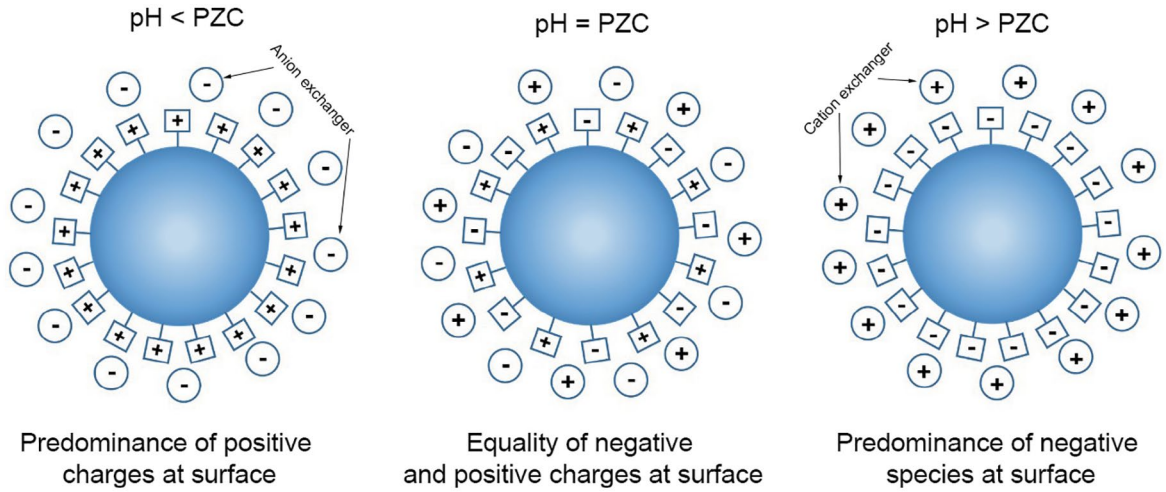


Fig. 6. Representation of predominant charge on the surface of adsorbent depending on pH.

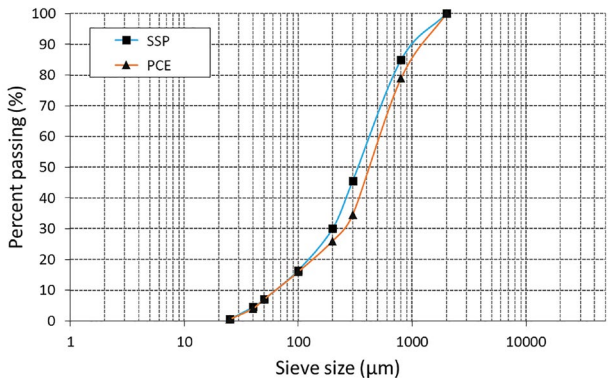


Fig. 7. Particle size distribution curve of SSP and PCP.

largest proportion of the sample. The percentage of fine particles (≤300 µm) is more than 85% and 79% for PCP and SSP, respectively.

The coefficient of uniformity ($C_u$) and the coefficient of curvature ($C_c$) are calculated from Eqs. (4) and (5) [47].

$$C_u = \frac{D_{60}}{D_{10}} \tag{4}$$

$$C_c = \frac{D_{30}^2}{D_{10} \times D_{60}} \tag{5}$$

where $D_{60}$, $D_{30}$ and $D_{10}$ are the particle diameters, corresponding to 60%, 30% and 10% finer on the cumulative particle size distribution curve, respectively.

The coefficient of uniformity ($C_u$) was used to classify the material as uniformly graded ($C_u > 5$) or poorly graded ($C_u < 5$). Hence, the coefficient of uniformity was 8.80 for SSP and 7.35 for PCP. Thus, the samples may be considered as uniformly graded. The coefficient of curvature ($C_c$) was 0.52 for SSP and 0.29 for PCP. The obtained results showed that these solids have a fine particle size distribution, which means that the particles may have a high porosity and surface area.

## 4. Conclusion

In order to predict their potential use in the adsorption process, the characterization of the materials is of extreme importance. In this work, the SSP and PCP were studied as promising candidates for heavy metals adsorption, highly available in Morocco and free of expense. XRD served to determinate the crystalline structure of the materials. FTIR analysis revealed the presence of carbonate ions in SSP and the functional groups (ketones, hydroxyl, carboxylic and phenolic) in PCP. The PZC was determined to be 7.97 and 5.62 for SSP and PCP, respectively. SEM analysis revealed the micro-rough texture of the material's surface. Their particle size analysis showed a fine particle size distribution.

The obtained results from this study can be considered when in view of the uses of those materials in the pollutants removal from wastewater. The understanding of the involved mechanisms is of great importance for the development of adsorption processes and can be a promising field for future research.

## References

[1] E. Worch, Adsorption Technology in Water Treatment, De Gruyter, Berlin, Boston, 2012.
[2] M.A.A. Wijayawardena, M. Megharaj, R. Naidu, Exposure, toxicity, health impacts, and bioavailability of heavy metal mixtures, Adv. Agron., 138 (2016) 175–234.
[3] V.K. Gupta, I. Ali, Water Treatment for Inorganic Pollutants by Adsorption Technology, in: Environmental Water, Elsevier, 2013, pp. 29–91.
[4] C. Palma, E. Contreras, J. Urra, M.J. Martínez, Eco-friendly Technologies based on banana peel use for the decolourization of the dyeing process wastewater, Waste Biomass Valor.. 2 (2011) 77–86.
[5] Y.C. Sharma, V. Srivastava, V.K. Singh, S.N. Kaul, C.H. Weng, Nano-adsorbents for the removal of metallic pollutants from water and wastewater, Environ. Technol., 30 (2009) 583–609.
[6] D. Sud, G. Mahajan, M.P. Kaur, Agricultural waste material as potential adsorbent for sequestering heavy metal ions from aqueous solutions - a review, Bioresour. Technol., 99 (2008) 6017–6027.
[7] D. Lubell, Are land snail a signature for the mesolithic-neolithic transition, Doc. Praehist., 31 (2004) 1–24.

[8] A. Kilic, H. Hafizoglu, I.E. Dönmez, I. Tümen, H. Sivrikaya, M. Reunanen, J. Hemming, Extractives in the cones of Pinus species, Eur. J. Wood Wood Prod., 69 (2010) 37–40.
[9] M. Momčilović, M. Purenović, A. Bojić, A. Zarubica, M. Randelovid, Removal of lead(II) ions from aqueous solutions by adsorption onto pine cone activated carbon, Desalination, 276 (2011) 53–59.
[10] N.A. Oladoja, Y.D. Aliu, Snail shell as coagulant aid in the alum precipitation of malachite green from aqua system, J. Hazard. Mater., 164 (2009) 1496–1502.
[11] M.R. Malekbala, S. Hosseini, S. Kazemi Yazdi, S. Masoudi Soltani, M.R. Malekbala, The study of the potential capability of sugar beet pulp on the removal efficiency of two cationic dyes, Chem. Eng. Res. Des., 90 (2012) 704–712.
[12] A. Shafiu Kamba, M. Ismail, T.A. Tengku Ibrahim, Z.A.B. Zakaria, Synthesis and characterisation of calcium carbonate aragonite nanocrystals from cockle shell powder (*Anadara granosa*), J. Nanomater., 2013 (2013). doi: 10.1155/2013/398357.
[13] S.W. Lee, Y.N. Jang, K.W. Ryu, S.C. Chae, Y.H. Lee, C.W. Jeon, Mechanical characteristics and morphological effect of complex crossed structure in biomaterials: fracture mechanics and microstructure of chalky layer in oyster shell, Micron, 42 (2011) 60–70.
[14] S.L. Mohd Abd Ghafar, M.Z. Hussein, Z. Abu Bakar Zakaria, Synthesis and characterization of cockle shell-based calcium carbonate aragonite polymorph nanoparticles with surface functionalization, J. Nanopart., 2017 (2017) 1–12. doi: 10.1155/2017/8196172.
[15] J.C. Kim, S.W. Lee, Y.N. Jang, Characteristics of the aragonitic Layer in adult oyster shells, *Crassostrea gigas*: structural study of myostracum including the adductor muscle scar, Evidence-Based Complementary Altern. Med., 2011 (2011). doi:10.1155/2011/742963.
[16] F. Marte, A. Péquignot, Shellmidden of Imiwaia I site (Beagle Channel, Argentina). Study of *Mytilus edulis* shell with FTIR-ATR, Anthropologie, 117 (2013) 135–160.
[17] A.P. Lim, A.Z. Aris, Continuous fixed-bed column study and adsorption modeling: removal of cadmium (II) and lead (II) ions in aqueous solution by dead calcareous skeletons, Biochem. Eng. J., 87 (2014) 50–61.
[18] N. Ouazene, M.N. Sahmoune, Equilibrium and kinetic modelling of astrazon yellow adsorption by sawdust: effect of important parameters, Int. J. Chem. React. Eng., 8 (2010) 151.
[19] B. Esteves, A. Velez Marques, I. Domingos, H. Pereira, Chemical changes of heat treated pine and eucalypt wood monitored by FTIR, Maderas. Cienc. y Tecnol., 15 (2013) 245–258.
[20] A.E. Ofomaja, E.B. Naidoo, S.J. Modise, Removal of copper(II) from aqueous solution by pine and base modified pine cone powder as biosorbent, J. Hazard. Mater., 168 (2009) 909–917.
[21] S. Dawood, T.K. Sen, Removal of anionic dye Congo red from aqueous solution by raw pine and acid-treated pine cone powder as adsorbent: equilibrium, thermodynamic, kinetics, mechanism and process design, Water Res., 46 (2012) 1933–1946.
[22] M. Calero, A. Pérez, G. Blázquez, A. Ronda, M.A. Martín-Lara, Characterization of chemically modified biosorbents from olive tree pruning for the biosorption of lead, Ecol. Eng., 58 (2013) 344–354.
[23] A.N. Kosasih, J. Febrianto, J. Sunarso, Y.H. Ju, N. Indraswati, S. Ismadji, Sequestering of Cu(II) from aqueous solution using cassava peel (*Manihot esculenta*), J. Hazard. Mater., 180 (2010) 366–374.
[24] C.-M. Popescu, M.-C. Popescu, G. Singurel, C. Vasile, D.S. Argyropoulos, S. Willfor, Spectral Characterization of Eucalyptus Wood, Appl. Spectrosc., 61 (2007) 1168–1177.
[25] R.F. do. Nascimento, F.W. de Sousa, V.O. Sousa Neto, P.B. Almeida Fechine, R.N. Pereira Teixeira, P. de T. C. Freire, M. Antonio, Biomass Adsorbent for Removal of Toxic Metal Ions From Electroplating Industry Wastewater, in: Electroplating, InTech, 2012, pp. 101–136.
[26] M. Poletto, H.L. Ornaghi Júnior, A.J. Zattera, Native cellulose: Structure, characterization and thermal properties, Materials (Basel), 7 (2014) 6105–6119.
[27] C.K. Jain, D.S. Malik, A.K. Yadav, Applicability of plant based biosorbents in the removal of heavy metals: a review, Environ. Process., 3 (2016) 495–523.
[28] S. Vigneswaran, H.H. Ngo, D.S. Chaudhary, Y.-T. Hung, Physicochemical Treatment Processes for Water Reuse, in: Physicochemical Treatment Processes, Humana Press, Totowa, NJ, 2005, pp. 635–676.
[29] M.N. Sahmoune, A.R. Yeddou, Potential of sawdust materials for the removal of dyes and heavy metals: examination of isotherms and kinetics, Desal. Wat. Treat., 57 (2016) 24019–24034.
[30] S.K. Bozbaş, Y. Boz, Low-cost biosorbent: Anadara inaequivalvis shells for removal of Pb(II) and Cu(II) from aqueous solution, Process Saf. Environ. Prot., 103 (2016) 144–152.
[31] G. Aditya, A. Hossain, Valorization of aquaculture waste in removal of cadmium from aqueous solution: optimization by kinetics and ANN analysis, Appl. Water Sci., 8 (2018) 68.
[32] S.L. Mohd Abd Ghafar, M.Z. Hussein, Y. Rukayadi, M.Z.A.B. Zakaria, Surface-functionalized cockle shell-based calcium carbonate aragonite polymorph as a drug nanocarrier, Nanotechnol. Sci. Appl., 10 (2017) 79–94.
[33] R.H. Gumus, I. Okpeku, Production of activated carbon and characterization from snail shell waste (Helix pomatia), Adv. Chem. Eng. Sci., 5 (2015) 51–61.
[34] Y.L. Hsieh, Chemical Structure and Properties of Cotton, in: Cotton, Elsevier, 2007, pp. 3–34.
[35] S. Park, J.O. Baker, M.E. Himmel, P.A. Parilla, D.K. Johnson, Cellulose crystallinity index: measurement techniques and their impact on interpreting cellulase performance, Biotechnol. Biofuels, 3 (2010) 10.
[36] L. Yuan, J. Wan, Y. Ma, Y. Wang, M. Huang, Y. Chen, The content of different hydrogen bond models and crystal structure of eucalyptus fibers during beating, BioResources, 8 (2012) 717–734.
[37] L. Segal, J.J. Creely, A.E. Martin, C.M. Conrad, An empirical method for estimating the degree of crystallinity of native cellulose using the X-ray diffractometer, Text. Res. J., 29 (1959) 786–794.
[38] Z. Ling, S. Chen, X. Zhang, K. Takabe, F. Xu, Unraveling variations of crystalline cellulose induced by ionic liquid and their effects on enzymatic hydrolysis, Sci. Rep., 7 (2017) 10230.
[39] A.D. French, Idealized powder diffraction patterns for cellulose polymorphs, Cellulose, 21 (2014) 885–896.
[40] H.L. Ornaghi Júnior, Á. de G.O. Moraes, M. Poletto, A.J. Zattera, S.C. Amico, Chemical composition, tensile properties, and structural characterization of the buriti fiber, Cellul. Chem. Technol., 50 (2016) 15–22.
[41] M. Poletto, V. Pistor, A. J., Structural Characteristics and Thermal Properties of Native Cellulose, in: Cellulose - Fundamental Aspects, InTech, 2013.
[42] M. Juned, K. Ahmed, M. Ahmaruzzaman, A review on potential usage of industrial waste materials for binding heavy metal ions from aqueous solutions, J. Water Process Eng., 10 (2016) 39–47.
[43] K. Karageorgiou, M. Paschalis, G.N. Anastassakis, Removal of phosphate species from solution by adsorption onto calcite used as natural adsorbent, J. Hazard. Mater., 139 (2007) 447–452.
[44] P. Somasundaran, G. Agar, The zero point of charge of calcite, J. Colloid Interface Sci., 24 (1967) 433–440.
[45] W. Zou, H. Bai, S. Gao, K. Li, Characterization of modified sawdust, kinetic and equilibrium study about methylene blue adsorption in batch mode, Korean J. Chem. Eng., 30 (2013) 111–122.
[46] V.S. Munagapati, V. Yarramuthi, S.K. Nadavala, S.R. Alla, K. Abburi, Biosorption of Cu(II), Cd(II) and Pb(II) by *Acacia leucocephala* bark powder: kinetics, equilibrium and thermodynamics, Chem. Eng. J., 157 (2010) 357–365.
[47] V. Dubois, N.E. Abriak, R. Zentar, G. Ballivy, The use of marine sediments as a pavement base material, Waste Manage., 29 (2009) 774–782.